On the transport properties in partially overlapping van der Waals junctions through a multi-scale investigation

Emmanuele Cannavò,[1] Damiano Marian,[1] Enrique González Marín,[2] Giuseppe Iannaccone,[1] and Gianluca Fiori[1, *]

[1]*Dipartimento di Ingegneria dell'Informazione, Università di Pisa, Via G. Caruso 16, 56122 Pisa, Italy*
[2]*Departamento de Electrónica y Tecnología de Computadores, Facultad de Ciencias,*
Universidad de Granada, Avenida de la Fuente Nueva S/N 18071 Granada, Spain

Van der Waals heterostructures are promising candidates for bringing the materials-on-demand paradigm into reality [F. Capasso, Science **235**, 172 (1987)], since their electrical properties can be engineered by playing on the several available degrees of freedom, as the number of layers, the materials and the order in which they are stacked. In the present work, we present *ab initio* and transport simulations of five different homo- and heterostructures based on two-dimensional materials, using a multi-scale computational platform to compute the out-of-plane transmission coefficients. This information can be relevant for a wide range of applications, from nanoscale devices to inkjet-printed circuits based on two-dimensional materials. Each structure has been investigated considering several parameters as the stacking sequence and orientation, as well as the different overlappings between the flakes. We have found that, while transmission across the junction is not significantly influenced by the degree of overlap between the flakes, the different stacking orientation plays a more relevant role.

I. INTRODUCTION

In recent years, the interest in two-dimensional (2D) materials has grown significantly, not only from a fundamental physical point of view, but also from the technological application perspective. Among their properties, the possibility of obtaining three-dimensional (3D) structures with ad-hoc characteristics by stacking layers of 2D crystals has been one of the most promising features. This has been referred to as the materials-on-demand paradigm[1–4], where atomically thin monolayers can be assembled together to form vertical heterostructures, held together by van der Waals interactions[5–7]. Graphene- and Transition Metal Dichalcogenide- (TMD) based heterostructures open new opportunities for electronic applications, where graphene acts as a semi-metal and TMDs offer a wide range of electronic properties, i.e. semiconducting, semimetallic and metallic[11–20], while providing new paths towards the goal of obtaining high-performance nanoscale devices.

The possibility of arranging layers of 2D materials one on top of the other opens new perspectives also in flexible and wearable electronics, where printing of inks based on 2D materials have been demonstrated as a very attractive alternative route towards low-cost, large-scale and eco-friendly fabrication of electronics device on both rigid and flexible substrates[10]. This approach allows the synthesis of complex heterostructures consisting of a large number of flakes with various degrees of overlapping and stacking sequences, forming a network of flakes. From this perspective, the study of out-of-plane transport across vertical homo- and heterostructures is of foremost importance, and numerical simulations can provide physical insights on the main mechanisms at play, while helping in identifying the best option in order to obtain working devices.

Transport in homo- and heterostructures is a recent research topic, as demonstrated by the relatively small number of publications in the field[21–23], some focusing on photodetection[24], steep-slope cold-source transistors[25], sandwitched structures[26] or transport through bilayer graphene regions[39]. The adopted computational methods are based either on Density Functional Theory (DFT), which presents serious limitations on the affordable system sizes, due to its computational cost, or on a tight-binding pseudo-empirical approach, with fewer computational limitations, but at the cost of reduced accuracy.

In order to properly study vertical transport, a flexible approach is needed *i*) to deal with variable flake sizes, up to several tens of nanometers (which are at the moment unmanageable by atomistic simulations), and *ii*) to accurately describe the inter-layer interaction, capturing the atomistic subtleties governing the coupling of the orbitals.

To this purpose, in the present work we investigate transport through vertical homo- and heterostructures of 2D materials by means of an accurate multi-scale platform that combines *ab-initio* DFT calculations, Maximally Localized Wannier Functions (MLWF) and the Non-Equilibrium Green's Functions (NEGF) formalism, thus providing an accurate description of the physics governing both interactions and transport between flakes, and the possibility of scaling the structures down to experimentally realizable sizes[27–31]. In particular, the proper Wannierization of the DFT structure allows us, by finely projecting the plane wave basis onto the dominant atomic orbital, to build a Hamiltonian with mono- and bilayer regions of arbitrary size along the transport direction. Here, we focus on homostructures of graphene, MoS_2 and WSe_2, and heterostructures of MoS_2-WSe_2 and graphene-MoS_2, considering two stackings for each structure and different overlapping lengths.

The article is organized as follows. In Sec. II, we briefly describe the adopted multi-scale approach, together with a decoupling procedure to obtain the monolayer Hamiltonian from the bilayer one, while retaining DFT accuracy. In Sec. III the studied structures and the results of the

calculations are presented and discussed. Finally, Sec. IV is about the conclusions we draw from our analysis.

II. MODEL

The chosen multi-scale method combines *ab-initio* DFT, Maximally Localized Wannier Functions (MLWF) and Non-Equilibrium Green's Functions (NEGF), inspired by the approaches proposed in Refs. 27-31. In Figure 1a, a schematic depiction of the system under study, comprising two partially overlapped flakes, is shown. In order to determine the transport properties of the structure, we first perform a DFT computation of the electronic structure of a bilayer geometry by means of the Quantum Espresso suite[32,33]. Next, we proceed with the Wannierization[34], i.e., we perform a change of basis in order to express the bilayer Hamiltonian in terms of MLWF. The correct Wannierization of the DFT Hamiltonian is crucial for the subsequent steps of our approach: one has to select the proper initial projections for the starting Wannier functions, opting for those orbital-like states that mostly contribute to the subset of bands one is interested in. In our case, we chose the bands close to the Fermi level, the ones more involved in the transport process. The orbital projections depend on the specific material under study: they, for example, can be inferred from the projected density of states, selecting the orbitals that mostly contribute to the total density of states in the desired energy range. For the systems examined here, we detail the chosen initial projections in App. B. As an example, it is well known that the conduction and valence bands of single layer MoS_2 are mainly due to the contribution of the five d orbitals of Mo and of the three p orbitals of S[35]; these projections are indeed a good initial choice for obtaining a proper Wannierization of the MoS_2 Hamiltonian.

Following the procedure described in App. B, one obtains a bilayer Hamiltonian of the form illustrated in Figure 1b and reported hereafter:

$$\mathcal{H} = \begin{pmatrix} \mathcal{H}_{BF} & \mathcal{H}_{OD} \\ \mathcal{H}_{OD}^* & \mathcal{H}_{TF} \end{pmatrix}. \qquad (1)$$

In Eq. (1), it is possible to identify three distinct blocks: 1) the upper diagonal block, which corresponds to the bottom flake ($\mathcal{H}_{BF}$), 2) the lower diagonal block, which corresponds to the top flake ($\mathcal{H}_{TF}$) and 3) the upper right and bottom left off-diagonal blocks (transpose conjugates), which correspond to the connections between the two flakes ($\mathcal{H}_{OD}$). This Hamiltonian encodes all the information required for describing transport in a partially overlapped system of 2D flakes. As a matter of fact, for the considered structures, we have tested that the separate diagonalization of the top flake and bottom flake sub-hamiltonians, i.e. $\mathcal{H}_{BF}$ and $\mathcal{H}_{TF}$, provide, with very good accuracy, the same bands of the corresponding isolated monolayers (except for an overall shift in energy); thus, the following relation holds:

$$\mathcal{H}_{BF/TF} \approx \mathcal{H}_{MB/MT} + \lambda \mathcal{I} \qquad (2)$$

where $\mathcal{H}_{MB/MT}$ is the Hamiltonian of the isolated bottom (MB) or top (MT) monolayer, $\mathcal{I}$ is the identity matrix and λ is a real number. It is important to underline that Eq. (2) is not general, but it must be verified case by case. The constant λ represents an overall energy shift in the Hamiltonian, affecting only the diagonal elements (i.e. the on-site energies).
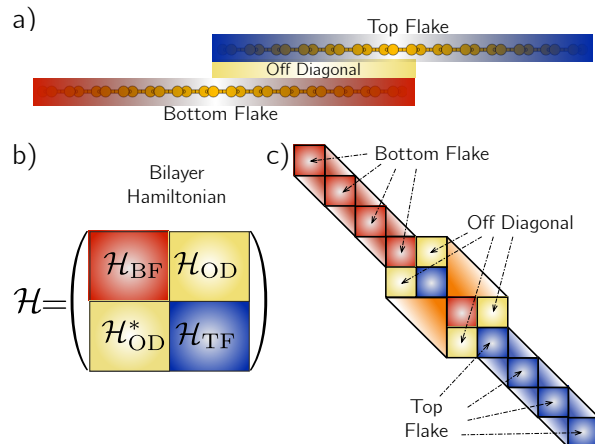

FIG. 1. (a) Schematic depiction of the considered structures: two flakes partially overlapped in the central region. (b) Schematic depiction of the bilayer Hamiltonian, with the three different blocks representing *i*) the top layer (upper left), *ii*) the bottom layer (lower right) and *iii*) the off-diagonal elements that connect the two layers. (c) Schematic depiction of the construction of the complete Hamiltonian with arbitrary single flake and overlapping regions. The triangles represents the connections between adjacent cells along the structure.

From Eq. (2), it is possible to construct the Hamiltonian of the entire device by selecting arbitrary sections of monolayer and overlap regions as schematically reported in Figure 1c. We finally compute the transmission coefficients by means of the non-equilibrium Green's functions formalism, implemented with the NanoTCAD ViDES package[36]. It is worth underlining that the present approach is able to retain the DFT level of accuracy, while simultaneously scaling the overlapping regions to several tens of nanometers (overcoming the size constrains of fully *ab-initio* approaches). As a drawback, we are neglecting boundary effects, which become increasingly more relevant the closer we come to the edges of the individual flake. Although this limitation can have an impact on small overlapping regions, it is not the case for the systems considered hereafter.

III. RESULTS AND DISCUSSION

III.1. Homostructures

Graphene — As a first example, we consider transport between partially overlapped flakes of graphene. Despite its importance, only few works[39,40] have addressed this issue through pseudo-empirical tight-binding meth-

ods. We consider two different stackings, namely AA and AB (see insets of Figure 2a and Figure 2b, respectively). We consider an experimental interlayer distance of 3.3 Å between the two graphene layers for both stackings[41]. In Figure 2a and Figure 2b we report the bandstructures close to the Dirac point along the path Γ — X: in the AA case we see a duplicate of the single layer graphene bands shifted in energy, while for the AB stacking we obtain two parabolic bands touching at the Dirac point[42]. These differences are expected to produce remarkably distinct transmission spectra for the two structures. Then, following the procedure outlined in Sec. II and recovering with a very good degree of precision the monolayer graphene bands from both the Hamiltonians of the AA and AB bilayers (see Fig. 2c), we compute the transmission for both stackings and for different overlapping lengths (from 12 nm to 50 nm) as shown in Figure 2d. As a first general observation, we note that the inter-flake transmission is always lower than the in-plane transmission in a monolayer. Looking at the two different stackings, we observe that for the AB case we have a transmission which is double, in the energy interval [-0.4,0.4] eV, with respect to the AA one. While a clear difference is observed for the different stackings, the behaviour is saturated with the overlapping length and we do not observe any significant difference in the transmission, which implies that the transmission length between the two flakes is smaller than 12 nm. It can be shown that this value emerges from local density of states considerations[43]. Furthermore, we note that around ± 0.48 eV, transmission for the AA stacking is partially suppressed, a feature that has been observed also experimentally[44].

TMDs — Next, we focus our attention on the vertical transport between partially overlapped flakes of MoS_2 and WSe_2. Both materials feature a direct band gap at the K point in the monolayer form (1.72 eV for MoS_2 and 1.29 eV for WSe_2), while the bilayers present an indirect band gap (from Γ in the valence band to K in the conduction band), of 1.26 eV for MoS_2 and of 1.10 eV for WSe_2. As for graphene, we consider two different stackings in the overlapping region, namely AA' and AB[37,45]; the two stackings are reported in Figures 3a and 3b, respectively. The interlayer distance, defined as the distance between the two nearest Sulfur/Selenium atoms, is set at 2.98 Å as reported in Ref. 17 for MoS_2 and to 3.24 Å as reported in Ref. 17 for WSe_2. In Figure 3c and Figure 3d, we show the comparison between the bands obtained from a monolayer structure and the ones extracted from the bilayer Hamiltonian of the AA' and AB stacking for MoS_2 and WSe_2, respectively. As for graphene, also in this case we observe a good agreement, especially near the conduction band minimum and the valence band maximum, i.e. in the energy range of interest for electronic applications. For WSe_2 calculations, we take into account spin-orbit coupling (SOC) (see App. A), which produces a splitting in the valence bands of the order of 0.4 eV in the monolayer; the energy separation disappears in the bilayer[17]. It is worth noticing that the monolayer WSe_2 Hamiltonian extracted from the bilayer
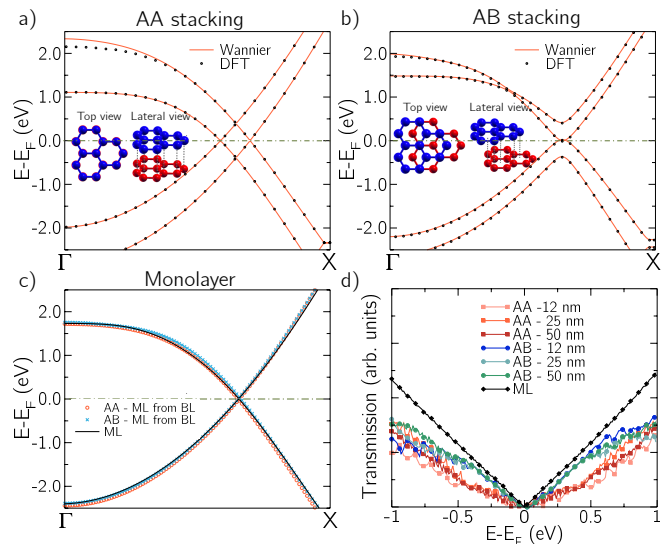

FIG. 2. Bilayer graphene bandstructure close to the Dirac point for (a) AA and (b) AB stacking obtained from DFT (black circles) and Wannier (red lines) simulations. (c) Comparison of monolayer (ML) graphene bandstructures: in red circles the one obtained with the diagonalization method of Sec. II applied to the AA bilayer (BL), in blue crosses the same for the AB bilayer, in black lines the isolated monolayer. (d) Electronic transmission spectrum of graphene for different degrees of superposition, for both AA and AB stacking, compared with the monolayer (ML) one.

one properly reproduces the bands splitting due to SOC (see Fig. 3d).

In Figure 3e the transmission coefficient for the AA' and AB cases for three different flake overlaps are shown for MoS_2, compared with the ones corresponding to the in-plane transport in a monolayer: we notice that the transmission in the valence band for the AA' stacking is increased by a factor of 2 with respect to the AB one. Therefore, we foresee a higher hole current in that energy window and we do not expect a significant difference between the two stackings as far as electron transport is concerned. In Fig. 3f, the transmission spectra of WSe_2 for the two considered configurations and for different overlapping lengths are shown: we observe that the AA' transmission is always lower than the AB one both in the valence and in the conduction bands. In this case, we expect the transmission to be influenced by the particular stacking for both electrons and holes. In both Figure 3e and Figure 3f, transmission is not significantly affected by the degree of superposition, suggesting again that the transfer length between the two layers is less than 12 nm, which is consistent with the literature[43].

III.2. Heterostructures

The method can be applied not only to interfaces between the same materials, but also to heterostructures. In the following, we study two different heterostructures:
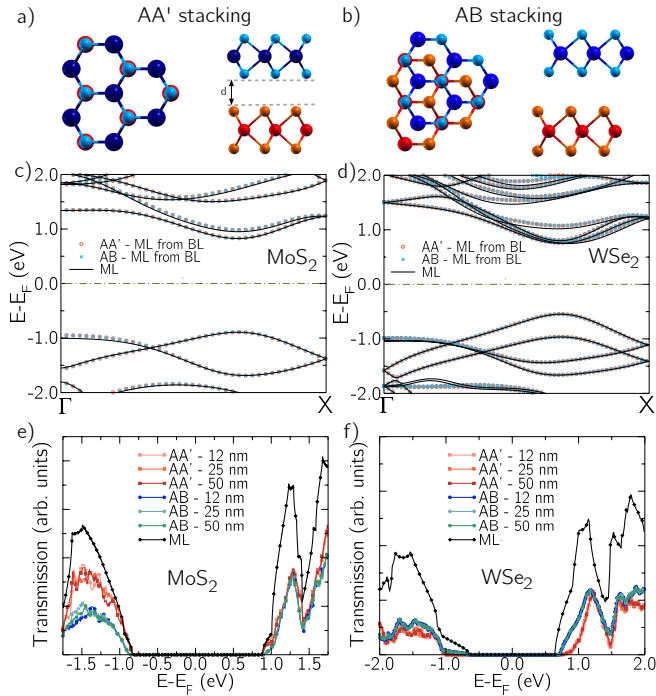
FIG. 3. Schematic depiction of the (a) AA' and (b) AB stacking for TMDs bilayers (top and lateral view). Comparison of monolayer (ML) MoS$_2$ (c) and WSe$_2$ (d) bandstructure along the Γ — X k-path: in red circles the one obtained with the diagonalization method of Sec. II applied to the AA' bilayer (BL), in blue crosses the same for the AB bilayer, in black lines for the isolated monolayer. Electronic transmission spectrum for MoS$_2$ (e) and WSe$_2$ (f) for different degrees of superposition, both for AA' and AB stacking, compared with the monolayer (ML) one.

WSe$_2$-MoS$_2$ and graphene-MoS$_2$.

WSe$_2$-MoS$_2$ heterostructure — In order to model the cell of the heterostructure, we separately relax the atomic position of the MoS$_2$ and WSe$_2$ monolayers, choosing a cell parameter of 3.26 Å; this value corresponds to the mean of the two relaxed cell parameters obtained from the homostructures in Sec. III. Afterwards, we build the heterostructure keeping the distance of $d = 3.37$ Å as reported in Ref. 20. The two stackings AA' and AB, previously described for TMDs homostructures, were considered for this bilayer as well. This WSe$_2$-MoS$_2$ heterostructure presents a direct bad gap of 0.60 eV. In Figure 4a and Figure 4b, we report the normalized projected density of states on band structure of the heterostructure bilayer: it is interesting to note that the conduction band minimum is mainly explained by the MoS$_2$ contribution, while the valence band maximum can be attributed to the WSe$_2$, as it is expected in a type-II (staggered gap) heterostructure.

To confirm that the procedure described in Sec. II can be applied also in this case, we report in Figures 4c and 4d the band profiles of the AA'/AB decoupled and isolated monolayers for MoS$_2$ and WSe$_2$, respectively. The overall agreement is better in the WSe$_2$ case, but for
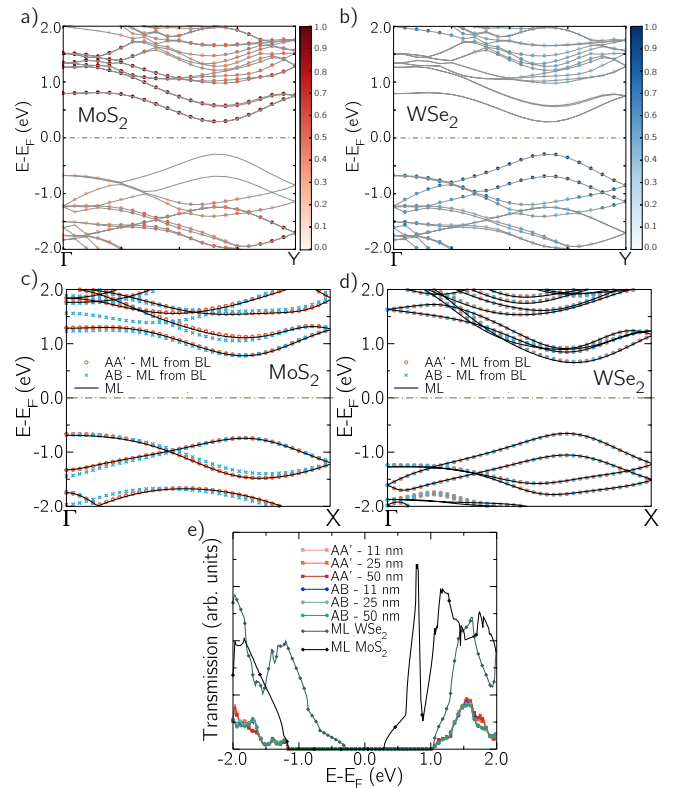

FIG. 4. Normalized projected density of states of the MoS$_2$ (a) and WSe$_2$ (b) states on the hetero-bilayer bands of the MoS$_2$-WSe$_2$ heterostructure. Comparison of monolayer (ML) MoS$_2$ (c) and WSe$_2$ (d) bandstructure along the Γ — X k-path: in red circles the one obtained with the diagonalization method of Sec. II applied to the AA' bilayer heterostuctures (BL), in blue crosses the same for the AB bilayer, in black lines the isolated monolayer. (e) Electronic transmission spectrum for MoS$_2$-WSe$_2$ heterostructure for different degrees of superposition, both for AA' and AB stacking, compared with the monolayer (ML) one for both isolated MoS$_2$ and WSe$_2$.

both materials the agreement for the bands closer to the gap is excellent. The transmission profiles (Figure 4e) are not affected by the different considered overlaps; furthermore, the AA' and AB stacking differ less than in the previous structures and the discrepancies are located far from the band gap. In general, we observe that the band alignment of the two materials produces an overall energy interval of 2.1 eV, where transmission is equal to zero: this is again due to the formation of a type II junction between WSe$_2$ and MoS$_2$. To confirm this, in Figure 4e, we also report the transmission coefficient for both MoS$_2$ and WSe$_2$ monolayers.

Graphene - MoS$_2$ heterostructure — The second considered heterostructure is composed by a monolayer graphene and MoS$_2$. In this case, it is not possible to perfectly commensurate the lattice parameters, because of the major difference between them. So, following Ref. 46, we consider a supercell consisting of 5x5 graphene and 4x4 MoS$_2$ ortorhombic elementary cells, as reported in Figure 5a. We have applied a tensile

strain on graphene of 3% while no strain has been applied to MoS_2. We take an interlayer distance, taken from the graphene layer to the nearest Sulfur atoms, of $d = 3.4$ Å, in agreement with the value reported in Ref. 44. The corresponding bandstructure is reported in Figure 5b, both for the DFT calculation and for the Wannierization; we notice an excellent agreement between the two. The distance between the Dirac point and the lowest conduction band is around 0.5 eV, which is in agreement with previous observations[47].This value of 0.5 eV means that, in equilibrium conditions, no significant charge transfer should be observed between the graphene and MoS_2 flakes, which is indeed true also in the experimental case[46]
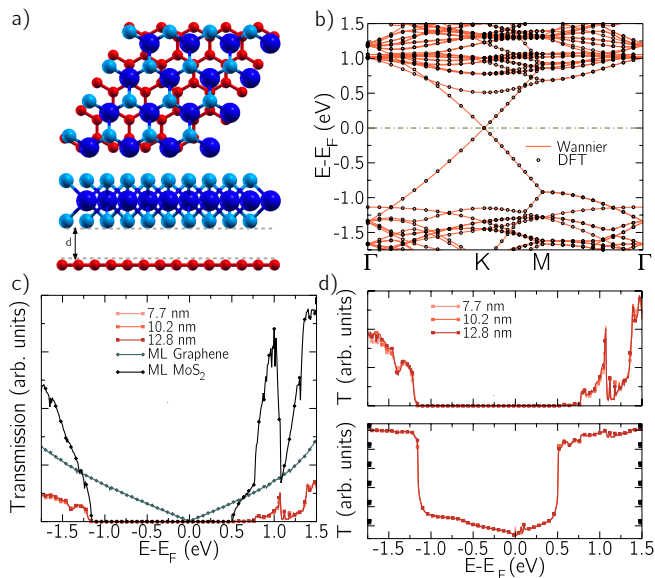

FIG. 5. a) Top and lateral view of the graphene-MoS_2 supercell consisting of 5x5 graphene cells and 4x4 MoS_2 cells. In the lateral view, the distance d between the graphene layer and the nearest Sulfur atoms is indicated. b) DFT (black circles) and Wannier (red solid lines) bandstructures along the Γ — K — M — Γ k path. c) Transmission coefficients for three different overlapping lengths (7.7, 10.2 and 12.8 nm). The transmissions for isolated monolayer (ML) graphene and MoS_2 are reported for reference. d) Same transmission coefficients as in c) in linear (top) and semi-logarithmic scale (bottom).

In Figure 5c, we report the transmission coefficient for three overlapping lengths (7.7 nm, 10.2 nm and 12.8 nm) of the structure reported in Figure 5a. In the same picture, as a reference, we also show the graphene and MoS_2 transmission coefficients: we can clearly observe that, with respect to the previously considered structures, the vertical transmission across the bilayers is largely reduced as compared to the monolayer case. Thus, for clarity, we isolated the heterostructure transmission plots and we show them in Figure 5d, in linear (top) and semi-logarithmic scale (bottom): we see that there is almost no difference for the three considered overlapping lengths meaning that the transmission length is smaller than 7.7 nm. This is interesting, as graphene has been pro-

posed as a candidate electrode in order to improve MoS_2-based devices[48], with the aim of reducing the contact resistance. From this perspective, our result shows that the electrode region can be made as small as few nanometers, and no significant loss due to the small overlapping region is expected. Our results are consistent not only with theoretical, but also with experimental findings[43], where the transfer length has been estimated to be 7 nm, considering drift transport in both graphene and MoS_2 with limited mobility.

IV. CONCLUSIONS

We have presented an accurate multi-scale method, capable of computing transport across 2D-materials-based homo- and heterostructures. In particular, we studied five structures: graphene, MoS_2 and WSe_2 as bilayers; MoS_2-WSe_2 and graphene-MoS_2. For each one, we considered two different stackings and various overlaps between the single flakes. We showed that the decoupling procedure for the stacked flakes provides accurate results, while exploiting the Hamiltonians of the respective isolated monolayers. From the analysis of the transport results, we conclude that, for all structures, transmission across the junctions is always smaller than in the monolayer case; also, the overlapping lengths do not affect the transmission coefficients significantly. In addition, we see that different stackings have a different impact on the transmission profiles. The method proposed can be extended to other materials and to combinations of them. The results obtained could be also exploited to further investigate a full van der Waals transistor, appropriately modeling the contacts and simulating transport in a self-consistent way; the peculiar properties of the TMDs in particular could be potentially used in the field of spin- and valleytronics, with the modeling of appropriate devices.

Appendix A: Computational Details

DFT calculations (relaxation, self-consistent field, bandstructure) were all carried out using the Quantum Espresso package. The chosen functional was always the GGA (Generalized Gradient Approximation) of Perdew, Burke and Ernzerhof (PBE)[38], while the pseudopotentials were ultrasoft ones for C, Mo and S modelling, and norm-conserving for W and Se. In all cases where WSe_2 was present, we included SOC effects by choosing the appropriate fully relativistic pseudopotential for W. In the self-consistent field simulations, wavefunction and density cutoff were respectively set at 40 and 400 Rydbergs for the graphene bilayer, 60 and 600 for the MoS_2 bilayer, 150 and 600 for the WSe_2 bilayer and the WSe_2-MoS_2 heterostructure, 50 and 500 for the graphene-MoS_2 heterostructure; k-points grids were 12x12x1 for the graphene bilayer, 6x6x1 for MoS_2 and WSe_2 homostructures and for their combined heterostructure, 3x3x1 for

the graphene-MoS_2 heterostructure. The relaxation calculation for the WSe_2/MoS_2 heterostructure used an energy and force convergence thresholds of 5×10^{-6} and 5×10^{-5} Rydbergs respectively, with values of 5×10^{-5} and 5×10^{-4} for the same quantity in the same kind of computation for the graphene-MoS_2 heterobilayer. Wannierization simulations were performed with version 2 of the Wannier90 software. Transmission simulations were run using the NanoTCAD ViDES software, in a flat potential condition and without employing self-consistency. The number of modes was fixed at 360 for all systems, apart from the graphene-MoS_2 heterostructure, where we chose 60, in order to account for a much bigger unit cell (5x4); energy ranges were 4 eV for the TMDs structures, 3 eV for graphene-MoS_2 and 2 eV for bilayer graphene; the number of principal layers was 2 for the graphene-MoS_2 heterostructures and 3 for all other bilayers.

Appendix B: Wannierization of the bilayer

The initial projections for the Wannierization of the bilayer structure are essential in order to have a bilayer Hamiltonian of the form reported in Eq. (1), i.e. one where it is possible to identify clearly the the diagonal blocks that can be associated the Hamiltonians of the bottom and top layers. The correct choice of the initial states is crucial, even if not sufficient, for satisfying the relation reported in Eq. (2), that must always be verified a posteriori for each system.

For both the AA and the AB bilayer graphene stackings, we selected one p_z orbital for each C atom and three sp^2 orbitals every two C atoms as initial guesses for the Wannier functions. For the Wannierization we used the disentanglement procedure described in Refs. 48 and 49, selecting 1 eV above the Dirac point as the highest value in the frozen energy window.

Regarding the TMDs homo- and heterostructures under analysis, i.e. MoS_2/WSe_2 homobilayers and the MoS_2-WSe_2 heterostructure, for the two considered stackings (AA' and AB), we chose five d orbitals for the transition metal atom (Mo/W) and three p orbitals for the chalcogen atom (S/Se) as initial projections for the Wannier functions. In all these cases, the bandstructure featured a convenient distinct subset in proximity of the Fermi level with the selected projections covering all bands included within it.

Finally, for the graphene-MoS_2 heterostructure we projected on the p_z orbital of each C atom and on the three sp^2 orbitals every two C atoms while on the five d orbitals for the Mo and on the s and the three p orbital for the S atoms. As in the case of the bilayer graphene, we used the disentanglement procedure, fixing the maximum energy in the frozen window 2.5 eV above the Dirac point. It is worth noting that in the Wannierization procedure it is useful, even if not mandatory, to assign different labels to atoms belonging to different layers, in order to easily single out the Wannier centres (i.e. bands) of each layer and clearly identify in the Hamiltonian reported in Eq. (1) the sub-matrices corresponding to the two layers. As a byproduct of the above described Wannierization procedure, one ends up with Wannier centres that are mainly localized around the atoms positions, so it is easy to identify the different Wannier functions belonging to different layers.

[*] gianluca.fiori@unipi.it

[1] K. S. Novoselov and A. H. Castro Neto, Two-dimensional crystals-based heterostructures: materials with tailored properties, Phys. Scr. **T146**, 014006 (2012).

[2] G. Iannaccone, F. Bonaccorso, L. Colombo, G. Fiori, Quantum engineering of transistors based on 2D materials heterostructures, Nature Nanotech **13** (2018).

[3] G. Fiori, F. Bonaccorso, G. Iannaccone, T. Palacios, D. Neumaier, A. Seabaugh, S. K. Banerjee, and L. Colombo, Electronics based on two-dimensional materials, Nature Nanotech **9**, 768 (2014).

[4] J.-H. Fu, A.-Y. Lu, N. J. Madden, C. C. Wu, J.-C. Chen, M.-H. Chiu, K. Hattar, J. A. Krogstad, S. S. Chou, L.-J. Li et al. Additive manufacturing assisted van der Waals integration of 3D/3D hierarchically functional nanostructures. Commun Mater **1**, 42 (2020).

[5] A. K. Geim and I. V. Grigorieva, Van der Waals heterostructures, Nature **499**, 419 (2013).

[6] K. S. Novoselov, A. Mishchenko, A. Carvalho and A. H. Castro Neto, 2D materials and van der Waals heterostructures, Science **353**, 461 (2016).

[7] X. Hu, L. Kou, and L. Sun, Stacking orders induced direct band gap in bilayer $MoSe_2$-WSe_2 lateral heterostructures, Sci. Rep. **6**, 31122 (2016).

[8] B. Amin, T. P. Kaloni, G. Schreckenbach, and M. S. Freund, Materials properties of out-of-plane heterostructures of MoS_2-WSe_2 and WS_2-$MoSe_2$, Appl. Phys. Lett. **108**, 063105 (2016).

[9] M.-H. Chiu, M.-Y. Li, W. Zhang, W.-T. Hsu, W.-H. Chang, M. Terrones, H. Terrones, and L.-J. Li, Spectroscopic Signatures for Interlayer Coupling in MoS_2-WSe_2 van der Waals Stacking, ACS Nano **8**(9), 9649 (2014).

[10] D. McManus, S. Vranic, F. Withers, V. Sanchez-Romaguera, M. Macucci, H. Yang, R. Sorrentino, K. Parvez, S. Son, G. Iannaccone et al., Water-based and Biocompatible 2D Crystal Inks: from Ink Formulation to All-Inkjet Printed Heterostructures, Nature Nanotech **12**, 343 (2017).

[11] W. Zhao, R. M. Ribeiro, M. Toh, . Carvalho, C. Kloc, A. H. Castro Neto and G. Eda, Origin of Indirect Optical

Transitions in Few-Layer MoS_2, WS_2, and WSe_2, Nano Lett. **13**, 5627 (2013).

[12] F. Wang, J. Wang, S. Guo, J. Zhang, Z. Hu and J. Chu, Tuning Coupling Behavior of Stacked Heterostructures Based on MoS_2, WS_2, and WSe_2, Sci Rep **7**, 44712 (2017).

[13] H. Terrones, F. López-Urías, and M. Terrones, Novel hetero-layered materials with tunable direct band gaps by sandwiching different metal disulfides and diselenides, Sci. Rep. **3**, 1549 (2013).

[14] S. Fang, S. Carr, M. A. Cazalilla, and E. Kaxiras, Electronic structure theory of strained two-dimensional materials with hexagonal symmetry, Phys. Rev. B **98**, 075106 (2018).

[15] J. Gusakova, X. Wang, L. L. Shiau, A. Krivosheeva, V. Shaposhnikov, V. Borisenko, V. Gusakov, and B. K. Tay, Electronic Properties of Bulk and Monolayer TMDs: Theoretical Study Within DFT Framework (GVJ-2e Method), Phys. Status Solidi A, 1700218 (2017).

[16] P. R. Bonneau, R. F. Jarvis Jr, and R. B. Kaner, Rapid solid-state synthesis of materials from molybdenum disulphide to refractories, Nature **349**, 510 (1991).

[17] N. Zibouche, P. Philipsen, A. Kuc, and T. Heine, Transition-metal dichalcogenide bilayers: Switching materials for spintronic and valleytronic applications, Phys. Rev. B **90**, 125440 (2014).

[18] A. Kumar and P.K. Ahluwalia, Electronic structure of transition metal dichalcogenides monolayers 1H-MX_2 (M = Mo, W; X = S, Se, Te), Eur. Phys. J. B **85**, 186 (2012).

[19] H. Liu, P. Lazzaroni, and C. Di Valentin, Nature of Excitons in Bidimensional WSe_2 by Hybrid Density Functional Theory Calculations, Nanomaterials **8**, 481 (2018).

[20] B. Amin, T. P. Kaloni, and U. Schwingenschlögl, Strain engineering of WS_2, WSe_2, and WTe_2, RSC Adv. **4**, 34561 (2014).

[21] X. Yuan, L. Tang, S. Liu, P. Wang, Z. Chen, C. Zhang, Y. Liu, W. Wang, Y. Zou, C. Liu et al., Arrayed van der Waals Vertical Heterostructures Based on 2D GaSe Grown by Molecular Beam Epitaxy, Nano Lett. **15**, 5, 3571 (2015).

[22] S.-J. Liang, B. Cheng, X. Cui, and F. Miao, Van der Waals Heterostructures for High-Performance Device Applications: Challenges and Opportunities, Adv. Mater. **32**, 1903800 (2020).

[23] J. Sonntag, J. Li, A. Plaud, A. Loiseau, J. Barjon, J. H. Edgar, and C. Stampfer, Excellent electronic transport in heterostructures of graphene and monoisotopic boron-nitride grown at atmospheric pressure, 2D Mater. **7**, 031009 (2020).

[24] D. Saha, A. Varghese, and S.Lodha, Atomistic Modeling of van der Waals Heterostructures with Group-6 and Group-7 Monolayer Transition Metal Dichalcogenides for Near Infrared/Short-wave Infrared Photodetection, ACS Appl. Nano Mater. **3**, 820 (2020).

[25] J. Lu, J. Pei, Y. Guo, J. Gong, and H. Li, A new opportunity for two-dimensional van der Waals heterostructures: making steep-slope transistors, Adv. Mater. **32**, 1906000 (2020).

[26] C. Xia, W. Xiong, W. Xiao, J. Du, L. Fang, J. Li, and Y. Jia, Enhanced Carrier Concentration and Electronic Transport by Inserting Graphene into van der Waals Heterostructures of Transition-Metal Dichalcogenides, Phys. Rev. Applied **10**, 024028 (2018).

[27] S. Bruzzone, G. Iannaccone, N. Marzari and G. Fiori, An Open-Source Multiscale Framework for the Simulation of Nanoscale Devices, IEEE Trans. Electron Devices **61**, 48 (2014).

[28] D. Marian, E. Dib, T. Cusati, E. G. Marin, A. Fortunelli, G. Iannaccone, and G. Fiori, Phys. Rev. Applied **8**, 054047 (2017).

[29] Á. Szabó, Ph.D. Thesis, ETH Zurich (2016).

[30] Á. Szabó, A. Jain, M. Parzefall, L. Novotny, and M. Luisier, Electron Transport through Metal/MoS_2 Interfaces: Edge- or Area-Dependent Process?, Nano Lett. **19**, 3641 (2019).

[31] Á. Szabó, S. J. Koester and M. Luisier, Ab-Initio Simulation of van der Waals $MoTe_2$–SnS_2 Heterotunneling FETs for Low-Power Electronics, IEEE Electron Device Letters **36**, 514 (2015).

[32] P. Giannozzi, S. Baroni, N. Bonini, M. Calandra, R. Car, C. Cavazzoni, D. Ceresoli, G. L. Chiarotti, M. Cococcioni, I. Dabo et al., QUANTUM ESPRESSO: a modular and open-source software project for quantum simulations of materials, J.Phys.: Condens.Matter **21**, 395502 (2009).

[33] P. Giannozzi, O. Andreussi, T. Brumme, O. Bunau, M. Buongiorno Nardelli, M. Calandra, R. Car, C. Cavazzoni, D. Ceresoli, M. Cococcioni et al., Advanced capabilities for materials modelling with Quantum ESPRESSO, J.Phys.: Condens. Matter **29**, 465901 (2017).

[34] A. A. Mostofi, J. R. Yates, G. Pizzi, Y. S. Lee, I. Souza, D. Vanderbilt, N. Marzari, An updated version of wannier90: A tool for obtaining maximally-localised Wannier functions, Comput. Phys. Commun. **185**, 2309 (2014).

[35] S. Haastrup, M. Strange, M. Pandey, T. Deilmann, P. S. Schmidt, N. F. Hinsche, M. N. Gjerding, D. Torelli, P. M. Larsen, A. C. Riis-Jensen, J. Gath, K. W. Jacobsen, J. J. Mortensen, T. Olsen, and K. S. Thygesen, The Computational 2D Materials Database: High-Throughput Modeling and Discovery of Atomically Thin Crystals, 2D Materials **5**, 042002 (2018).

[36] http://vides.nanotcad.com.

[37] J. He, K. Hummer, and C. Franchini, Stacking effects on the electronic and optical properties of bilayer transition metal dichalcogenides MoS_2, $MoSe_2$, WS_2 and WSe_2, Phys. Rev. B **89**, 075409 (2014).

[38] J. P. Perdew, K. Burke, and M. Ernzerhof, Generalized gradient approximation made simple, Phys. Rev. Lett. **77**, 3865 (1996).

[39] H. Z. Olyaei, P. Ribeiro, and E. V. Castro, Transmission across a bilayer graphene region, Phys. Rev. B **99**, 205436 (2019).

[40] S. Bruzzone, D. Logoteta, G. Fiori, and G.Iannaccone, Vertical transport in graphene-hexagonal boron nitride heterostructure devices, Sci Rep **5**, 14519 (2015).

[41] G. E. Bacon, The Interlayer Spacing of Graphite, Acta Cryst. **4**, 558 (1954).

[42] A.V. Rozhkova, A.O. Sboychakova, A.L. Rakhmanova, Franco Noria, Electronic properties of graphene-based bilayer systems, Physics Reports **648**, 1 (2016).

[43] D. S. Schneider, E. Reato, L. Lucchesi, Z. Wang, A. Piacentini, J. Bolten, D. Marian, E. G. Marin, A. Radenovic, Z. Wang et al., MoS_2/graphene Lateral Heterostructure Field Effect Transistors, DRC 2021 (to be published).

[44] M. M. Furchi, A. Pospischil, F. Libisch, J. Burgdo, and T. Mueller, Photovoltaic Effect in an Electrically Tunable van der Waals Heterojunction, Nano Lett. **14** 4785 (2014).

[45] T. Cusati, A. Fortunelli, G. Fiori, and G. Iannaccone, Stacking and interlayer electron transport in MoS_2, Phys. Rev. B **98**, 115403 (2018).

[46] D. Pierucci, H. Henck, J. Avila, A. Balan, C. H. Naylor, G. Patriarche, Y. J. Dappe, M. G. Silly, F. Sirotti,

A. T. C. Johnson et al., Band Alignment and Minigaps in Monolayer MoS2-Graphene van der Waals Heterostructures, Nano Lett. **16**, 4054 (2016).

[47] S. Singh, C. Espejo, and A. H. Romero, First-principles investigation of graphene/MoS 2 bilayer heterostructures using Tkatchenko-Scheffler van der Waals method, Phys. Rev. B **98**, 155309 (2018).

[48] W.-S. Leong, X. Luo, Y. Li, K. H. Khoo, S. Y. Quek, and J. T. L. Thong, Low Resistance Metal Contacts to MoS_2 Devices with Nickel-Etched-Graphene Electrodes, ACS Nano **9**, 1, 869 (2015).

[49] N. Marzari, A. A. Mostofi, J.n R. Yates, I. Souza, and D. Vanderbilt, Maximally localized Wannier functions: Theory and applications, Rev. Mod. Phys. **84**, 1419 (2012).

[50] I. Souza, N. Marzari, and D. Vanderbilt, Maximally localized Wannier functions for entangled energy bands, Phys. Rev. B **65**, 035109 (2001).